Journal of
Materials Chemistry A

Materials for energy and sustainability

Accepted Manuscript

This article can be cited before page numbers have been issued, to do this please use: X. Wang, J. Xie, Q. Zhao and Q. Sun, *J. Mater. Chem. A*, 2024, DOI: 10.1039/D4TA03129F.

ROYAL SOCIETY OF CHEMISTRY

rsc.li/materials-a

View Article Online
DOI: 10.1039/D4TA03129F

COMMUNICATION

Self-supported antimony tin oxide anode with Sb segregation promoted atrazine removal

Received 00th January 20xx,
Accepted 00th January 20xx

DOI: 10.1039/x0xx00000x

Xue Wang,[a] Jia-Fang Xie,*[a,b] Quan-Bao Zhao,*[a,b] Qian Sun[a,b]

Electrochemical oxidation is a sustainable approach to remove persistent organic pollutants, while suffers from slow reaction transfer. Herein, a robust self-supported antimony tin oxide anode was developed by compaction-sintering process with engineer fiber as pore-forming reagent and second binder. The obtained EF-ATO anode presented Sb segregation induced built-in electric field (BIEF), realizing 95% removal efficiency of atrazine (ATZ) in 30 min. Kinetics, Kelvin probe force microscopy, and *in-situ* EPR included analysis revealed that BIEF accelerated reaction charge transfer for the co-generation of three reactive oxygen species, contributing to the highly efficient ATZ removal. Furthermore, robust EF-ATO exhibited low energy consumption, high durability over 10-times cycling tests, and wide applicability in pH and pollutant type. Thus, EF-ATO possessed high potential as a promising candidate for the persistent organic pollutants' eco-removal. This work provides an approach for designing robust self-supported metal oxide-based anodes and reveals an electrochemical oxidation process promoted by doping metal segregation induced BIEF.

Introduction

Clean water is vital for the human survival and production, but is threatened by persistent organic pollutants, pesticides included. By exemplifying, atrazine (ATZ), an extensively used pesticide, has been detected to widely dispersed in multiple water bodies.[1,2] However, traditional biological treatment and physical methods can not effectively remove them.

Several technologies have been developed to remove ATZ included persistent organic pollutants, among which electrochemical oxidation (EO) has attracted increasing attention.[3] It has advantages of high controllability and efficiency,[4] minimal secondary pollution and aeration, and wide applicability to diversified persistent organic pollutants.[5,6] Reactive oxygen species (ROS), such as hydroxyl radicals (•OH), superoxide radicals ($\bullet O_2^-$), and singlet oxygen ($^1O_2$), generated in EO process can effectively remove and even mineralize persistent organic pollutants due to their high oxidation potentials.[7] ROS generation performance heavily depends on the anode.[8] However, on widely studied metal oxide based anodes, sluggish charge transfer in metal oxides often limited the ROS generation and pollutants removal efficiency.[9]

There are two strategies to prepare EO anodes with metal oxide catalyst powder: (1) coating catalyst contained ink onto the planar-structured substrate layer-by-layer and repeatedly annealing to be a planar catalyst coated anode,[10] and (2) compacting catalyst contained powder mixture in a mould and one-time sintering to be a 3D self-supported porous anodes.[11] The former one costs less mass of catalyst but requires an interlayer, which usually contains Pt, Ru, and Ir, to even and stabilize catalyst powder on anodes.[12,13] In contrast, the latter one requires pore-forming (polymethacrylate, carbon fiber (CF), starch, etc.)[11,14,15] and binder reagents (paraffin oil, polyacrylic acid, chitosan, etc.)[16-18] addition into more catalyst mass to shape. After sintering, self-supported anodes gain uniform composition and porous structure because pore-forming and binder reagents decompose during sintering. Freestanding SnO_x/La-Sb anode and Ti_4O_7 anodes[19,20] prepared by this compaction-sintering strategy showed effectively and rapidly remove moxifloxacin and 4-chlorophenol, respectively. Despite of these great achievements, the removal efficiency and kinetics have still been limited by sluggish charge transfer in metal oxides. When second metal was doped to increase the conductivity, how doping metal can improve reaction charge transfer has not been paid sufficient attention.

In this work, we take Sb-doped SnO_2 (ATO), a widely studied metal oxide EO catalyst, as a model catalyst to develop a robust and effective self-supported ATO anode by a double

[a] CAS Key Laboratory of Urban Pollutant Conversion, Institute of Urban Environment, Chinese Academy of Sciences, Xiamen, 361021, China. E-mail: jfxie@iue.ac.cn; qbzhao@iue.ac.cn.
[b] University of Chinese Academy of Sciences, Beijing, 100049, China.

Electronic Supplementary Information (ESI) available:. See DOI: 10.1039/x0xx00000x

binder strategy. Polypropylene engineer fiber (EF) was chosen as pore-forming reagent because it provides extra binder function besides of low cost and density, easy decomposition without residue under low temperature, and hard-elastic properties. EF are widely applied in construction industry because of forming a scrambled support system in cement. The structural properties of obtained EF-ATO anode was studied with the focus on Sb segregation driven by 1000°C sintering. The EO performance of EF-ATO anode for ATZ removal was investigated. Under optimized conditions, the durability and applicability of EF-ATO anode were evaluated. The effect of Sb segregation on the excellent EO performance was revealed with multiply techniques. Finally, the intermediates of ATZ degradation with EF-ATO anode and their ecotoxicity were analysed.

Results and discussion

By compaction and 1000°C sintering with EF, some micron-level cavities derived from EF could be observed without residue in EF-ATO anode (Fig. 1a). High resolution scanning electron microscope revealed the size of ATO particles grew from about 20 nm (Fig. S1) to nearly 80 nm in EF-ATO (Fig. 1a). X-ray diffraction (XRD) patterns of these two materials shared the same peaks located at 26.58°, 33.91°, 37.95°, 51.80°, and 54.76° (Fig. 1c), in good agreement with (110), (101), (200), (211) and (220) crystal planes of the tin oxide phase (PDF No. 01-088-2348), respectively. The higher and narrower peaks of EF-ATO proved its better crystal structure after sintering, which would facilitate charge transfer. Meanwhile, the specific surface area reduced by nearly 80% and micropores and small mesopores almost disappeared (Fig. S2 and Table. S1), indicating the smoother surface of larger ATO particles in EF-ATO. Notably, the EF-ATO anode possessed higher integrity and mechanical strength over the ATO anode with CF as pore-forming reagent (CF-ATO, Fig. S3 and Table S2), proving the advantage of EF with extra binder function. This feature would allow self-supported EF-ATO to adjust various device configurations and tough operation conditions for the complicated application. Additionally, although CF-ATO showed the similar N_2 adsorption-desorption isotherm with EF-ATO, carbon fiber residue could be observed (Fig. S4), possibly due to the incomplete decomposition of CF with much higher decomposition temperature than EF.

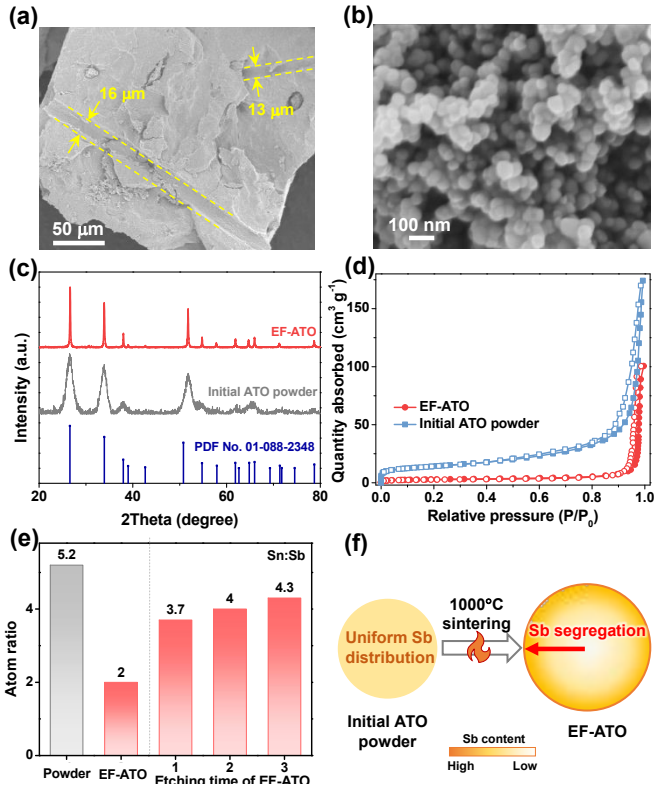

Fig. 1 The structural properties of EF-ATO. (a, b) SEM images. (c) XRD patterns. (d) N_2 adsorption-desorption isotherms. Initial ATO powder was shown as comparison. (e) Surface Sn:Sb atomic ratio and in-depth Sn:Sb from XPS. (f) Illustration of heat-driven Sb segregation in EF-ATO.

The survey X-ray photoelectron spectroscopy (XPS) spectra of EF-ATO anode showed the presence of Sn, Sb, and O, besides of C from adsorbed CO_2 (Fig. S5a). C 1s was calibrated to 284.8 eV (Fig. S5b) before fitting high-resolution XPS spectra of Sn, Sb, and O. Based on the fitting results, the surface atomic ratio of Sn:Sb was 2.0 for EF-ATO (Fig. 1e), apparently smaller than initial ATO powder (5.2) and similar with CF-ATO anode (2.2), indicating 1000°C sintering driving this change. The further depth-profiling XPS spectra of EF-ATO presented the gradually concentrated Sb from inner part to the surface, proving Sb segregation driven by 1000°C sintering. Besides, the relative content of oxygen vacancy was firstly evaluated by calculating the area ratio of adsorbed oxygen (O_{ad}) to lattice oxygen (O_L) species.[21] Oxygen vacancy content for EF-ATO was calculated to be three-times higher than initial ATO, nearly opposite to surface Sn:Sb ratio, implying that 1000°C sintering generated oxygen vacancy on ATO.[22]. The EPR results further confirmed the enhanced oxygen vacancy content in EF-ATO over initial ATO powder (Fig. S6). The oxygen vacancy would tune the metal-O bonds by offering unsaturated coordination and optimize the interactions between ATO and water included oxygen-containing species, benefiting EO process.[23,24] Therefore, EF-ATO anode prepared by 1000°C sintering with EF as pore-forming reagent possessed Sb segregation and higher crystalline.

The EO properties of EF-ATO anode were investigated with ATZ as a typical persistent organic pollutant. Commercial boron doped diamond (BDD) and Ti mesh loaded ATO particles (ATO@Ti) were also examined as comparison. As shown in Fig. 2a, EF-ATO anode presented the highest removal efficiency of about 95% at 30 min and 99.3% at 60 min. As comparison, commercial BDD and ATO@Ti anodes showed a much lower removal efficiency of 79% and 61% at 60 min for ATZ. Correspondingly, EF-ATO held the higher value of ATZ removal rate constant as 0.086 min^{-1} (Fig. 2b) over BDD (0.026 min^{-1})

View Article Online
DOI: 10.1039/D4TA03129F

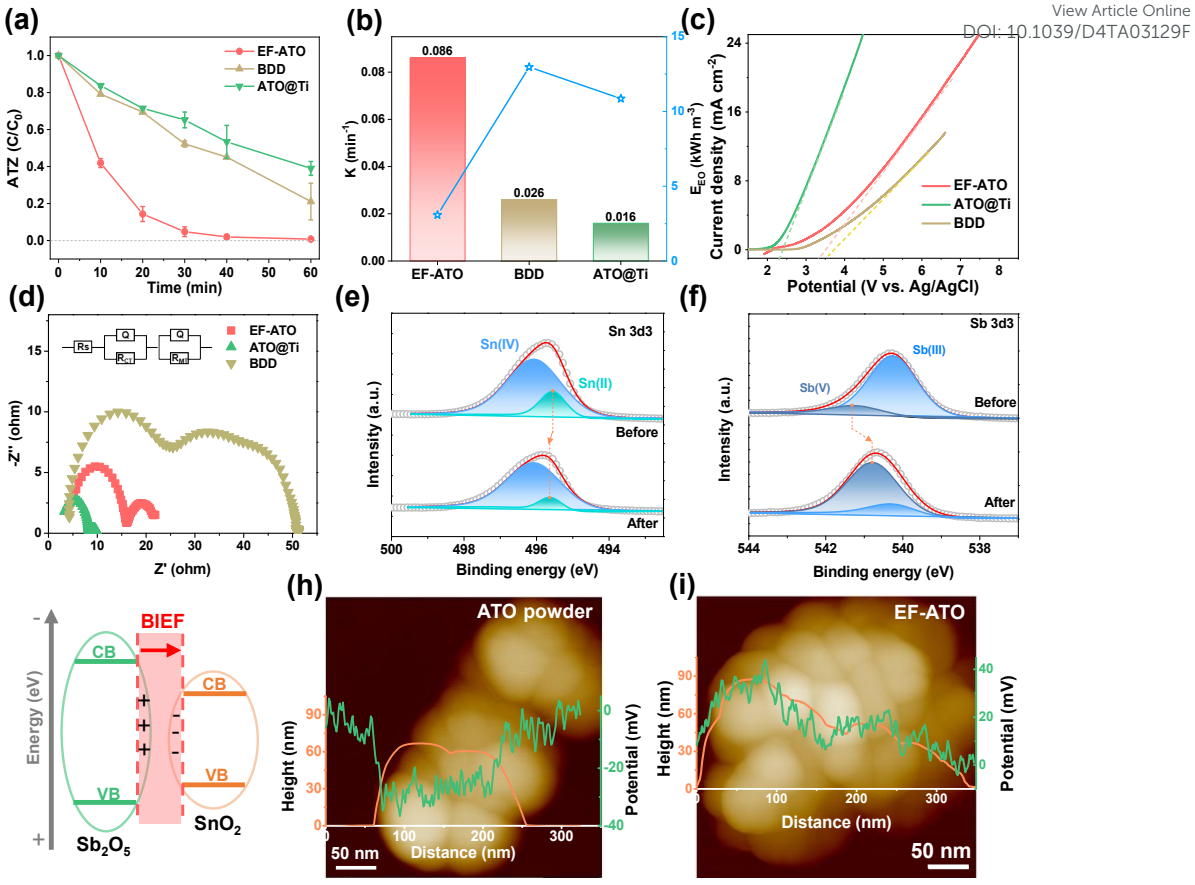

Fig. 2 EO performance for ATZ removal on EF-ATO. (a) ATZ removal rate, (b) the corresponding removal rate constant and energy consumption. (c) LSV curve in 0.1 M Na_2SO_4. (d) EIS in 0.1 M Na_2SO_4. Commercial BDD and ATO@Ti ware also shown as comparison. High resolution XPS of (e) Sn 3d3 and (f) Sb 3d3. (g) The illustration of BIEF between Sb_2O_5 and SnO_2. KPFM image with linear height and surface potential distribution for (h) initial ATO powder and (i) EF-ATO. If not specified, experimental conditions: C_0 = 20 mg L^{-1}, current density = 10 mA cm^{-2}, pH = 6, and Na_2SO_4 concentration = 0.1 M.

and ATO@Ti anode (0.016 min^{-1}). Notably, this high-rate removal of ATZ on EF-ATO anode exceeds most of recent anodes (Table S3). Furthermore, the energy consumption of the EF-ATO anode for ATZ removal was only 3.08 kWh m^{-3}, much lower than that of BDD and commercial ATO@Ti. These results demonstrated the advantages of self-supported EF-ATO over powder coated ATO@Ti, which has also been reported by many other electrochemical reactions.[25]

To understanding the electro-kinetics of EF-ATO anode, linear scanning voltammetry (LSV) was conducted firstly to evaluate the oxygen evolution potential (OEP). The high OEP can significantly reduce side reaction of oxygen evolution, and thus enhance the generation of ROS, benefiting the ATZ removal capacity and energy efficiency.[26] As shown in Fig. 2c, the OEP of EF-ATO anode was 3.36 V, which is very close to the BDD (3.50 V) and far beyond ATO@Ti (2.35 V). Thus, EF-ATO is suggested to exhibit the superior performance of generating ROS similar to BDD and over ATO@Ti. Furthermore, the electrochemical impedance spectroscopy (EIS) study can reveal the impedance properties of the electrodes, specially reaction charge transfer resistance (R_{CT}) that is highly related to EO performance. According to the EIS curves, EF-ATO possessed an apparently smaller semicircle than BDD (Fig. 2d). Further fitting analysis showed that the R_{CT} of EF-ATO was 6.78 Ω, lower than that of BDD (30.12 Ω) and the close to ATO@Ti of 5.78 Ω (Table S4).

XPS characterization of EF-ATO after EO process was carried out to investigate the possible variation of atom ratio and valence of metal elements. After C 1s calibrated to 284.8 eV, high-resolution spectra of Sn 3d and Sb 3d&O1s were fitted (Fig. S7). Surface atom ratio of Sn:Sb slightly increased to 2.5, suggesting the stable existence of Sb segregation in EF-ATO. Interestingly, the location of Sn(II) peak moved to the higher binding energy and meanwhile Sb(V) peak moved negatively, suggesting the electron transfer from Sn(II) to Sb(V) during EO process. The electron transfer increased the ratio of Sb(V) in Sb and Sn(IV) in Sn that would benefit the ROS generation and ATZ removal by EO process with EF-ATO (Fig. S8). Besides, oxygen vacancy slightly increased after EO process (Fig. S9), suggesting its stable existence. Moreover, Sb segregation induced the concentrated Sb_2O_5-SnO_2 heterojunction structure on the surface over the inner part. Sb_2O_5-SnO_2 heterojunction would generate the built-in electric field (BIEF) between them (Fig. 2g), facilitating the charge transfer. Kelvin probe force microscopy (KPFM) measurement was further applied to measure the surface potential of ATO

View Article Online
DOI: 10.1039/D4TA03129F

particles, which is highly related to the built-in electric field (BIEF) strength.[27] According to KPFM results, pure tin oxide without Sb doping had the weakest BIEF strength (Fig. S10) and initial ATO with uniform Sb doping had a stronger BIEF than pure tin oxide (Fig. 2h). After 1000°C sintering, EF-ATO with Sb segregation showed the strongest BIEF strength (Fig. 2i). By accelerating the charge transfer and tuning intermediates adsorption for electrochemical reactions, the enhanced BIEF would promote ROS generation by EO process on EF-ATO anode.[22,28]

Influence factors on the EO process with EF-ATO were further studied. As shown in Fig. S11a, four binder contents during EF-ATO preparation made a slight of difference in ATZ removal efficiency. 5% binder content achieving the highest removal rate constant of 0.086 min^{-1} (Fig. S11b) was thus fixed for the following investigation of other influence factors. The electrolyte concentration affected ATZ removal efficiency a bit when it was as low as 0.02 mol L^{-1} (Fig. 3a). When electrolyte concentration gradually increased from 0.05to 0.15 mol L^{-1}, ATZ removal efficiencies at 60 min were nearly the same. While the removal rate constant achieved the highest value of 0.086 min^{-1} with 0.1 M electrolyte concentration (Fig. S11c). Thus, 0.1 M electrolyte would provide sufficient conductivity for this EO system with EF-ATO anode.[29] Increasing the initial pH of electrolyte from 3 to 11 showed slight influence on ATZ removal efficiency by EO process with EF-ATO (Fig. 3b) but played an obviously negative role in removal rate constant (Fig. S11d). The would be possibly ascribed to the enhancement of ROS generation in acid solution, as reported by previous works.[30] Taking cost and removal efficiency into consideration together, initial pH of 6 was chosen as the optimized one. Current density gradually increased from 5 to 15 mA cm^{-2} resulted in the tiny improvement of ATZ removal efficiency (Fig. S11e). The removal rate constant grew from 0.054 min^{-1} to 0.125 min^{-1} as the current density increased (Fig. 3c). Up to 96.9% ATZ could be removed in 30-min electrolysis at the current density of 15 mA cm^{-2}. However, when energy consumption was also taken into consideration, current density of 10 mA cm^{-2} would be the better choice with the lowest energy consumption to obtain one of the highest removal efficiencies in 60 min. Thus, 5% binder content, 0.1 M Na_2SO_4 solution with pH of 6, current density of 10 mA cm^{-2}, and 60-min electrolysis were chosen as the optimized conditions for the following experiments.

The EO properties of EF-ATO for more kinds of persistent organic pollutants ware also evaluated. EO system with EF-ATO presented excellent performance of removing bisphenol A (BPA), levofloxacin (LFX), sulfadiazine (SDZ), and tetracycline (TC) (Fig. 3d and S11f). These results suggest the promising application of EF-ATO in the efficient removal of more kinds of persistent organic pollutants. Finally, ten-times consecutive removal experiment showed highly stable removal efficiency of ATZ throughout the ten-times experiments (Fig. 3e). Therefore, robust EF-ATO could remove persistent organic

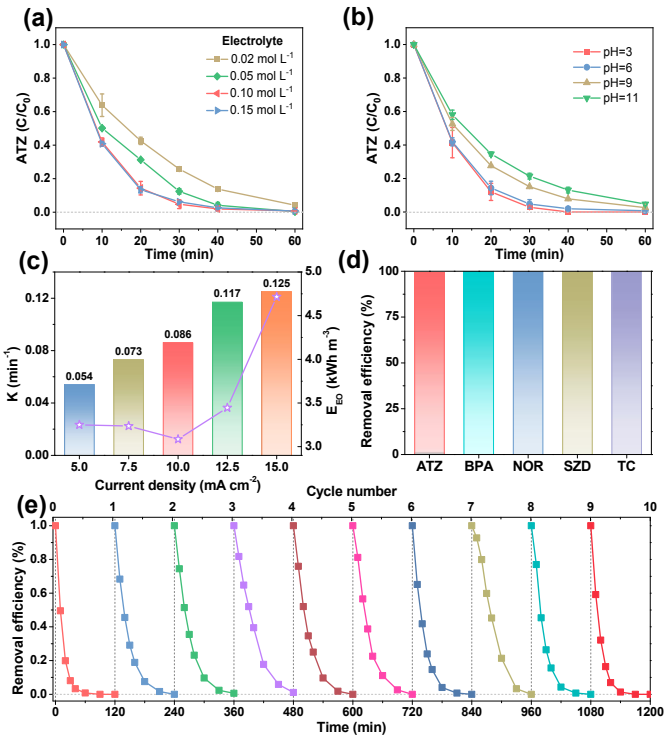

Fig. 3 Influence factors of ATZ removal on EF-ATO anode. Removal efficiency under a series of electrolyte (a) concentration and (b) pH. Removal rate constant and E_{EO} at a series of current densities. (d) Removal efficiency of different pollutants. (e) Recyclability of EF-ATO anode for ATZ removal. If not specified, experimental conditions: C_0 = 20 mg L^{-1}, j = 10 mA cm^{-2}, pH = 6, and Na_2SO_4 concentration = 0.1 M.

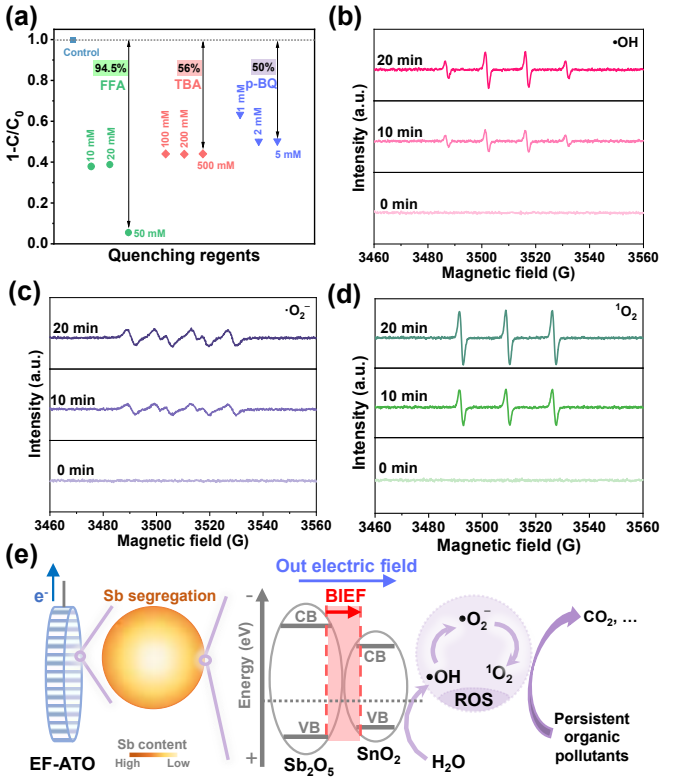

Fig. 4 ROS determination. (a) Quenching tests with TBA, FFA, and p-BQ, respectively. *In-situ* EPR spectra of (b) •OH, (c) $•O_2^-$, and (d) $^1O_2$. (e) Illustration of EF-ATO with Sb segregation enhanced EO process for persistent organic pollutants removal.

pollutants with high rate, high durability, low energy consumption, and wide applicability in pH and pollutant type.

To explore the possible ROS in the EO process on EF-ATO, the quenching experiments with three concentrations of quenching reagent were carried out firstly. Tert-butanol alcohol (TBA), furfuryl alcohol (FFA), and para-benzoquinone (p-BQ), respectively, were added into the electrolyte before the EO process took place (Fig. S12).[31] As depicted in Fig. 4a, ATZ removal efficiency was the most sensitive to the concentrated addition of FFA, as 50 mM FFA addition resulted in negligible removal of ATZ. TBA and p-BQ additions also decrease the ATZ removal efficiency up to around 50%. Their sum exceeded 100%, possibly owing to the complicated interconversion of ROS.[32] *In-situ* EPR further confirmed the characteristic signals of DMPO-• OH, DMPO-•O_2^-, and TEMP-$^1O_2$ and that their intensities improved as the electrolysis time going by (Figs. 4b-d). The relative contributions of three ROS to ATZ removal were evaluated with quenching experiments based on the equations in Supporting Information. Accordingly, •OH, •O_2^-, and $^1O_2$ contributed 30.8%, 48.7%, and 20.5%, respectively, to ATZ removal. These results demonstrated the co-generation of •OH, •O_2^-, and $^1O_2$ in the EO process, which could ascribe to the effective removal of multiply persistent organic pollutants for differed ROS has their respective dominant reaction activity to differed typical pollutant structures.

Finally, based on 19 intermediates of ATZ degradation identified by UPLC-MS/MS system with triple quadrupole mass spectrometer (Fig. S13 and Table S5), the possible 3 mainly pathways of ATZ removal in EO process with EF-ATO were proposed (Fig. S14). There were 6 reactions involved, including dechlorohydroxylation, dealkylation, dehydroxylation, alkyl hydroxylation, and hydroxylation reactions. To comprehensively evaluate the potential ecotoxicity of these intermediate products, the QSAR method combined with T.E.S.T was applied. According to the evaluation of acute toxicity, bioaccumulation factor, developmental toxicity, and mutagenicity of ATZ and 19 degradation intermediates (Fig. S15), the ecotoxicity of ATZ could be efficiently decreased by the EO process with EF-ATO. Thus, the mechanism of EF-ATO with Sb segregation enhancing the eco-removal of persistent organic pollutants by EO process was illustrated in Fig. 4e. On robust EF-ATO, Sb segregation induced BIEF enhanced reaction electron transfer in electrochemical water oxidation for ROS generation. All of •OH, •O_2^-, and $^1O_2$ played the important role in the robust eco-removal of persistent organic pollutants.

Conclusions

This work describes a self-supported EF-ATO anode with Sb segregation synthesized using a double binder strategy for persistent organic pollutant removal by EO process. EF-ATO possessed enhanced build-in electric field driven by Sb segregation, facilitating charge transfer and promoting the generation of •OH, •O_2^-, and $^1O_2$ in EO. Accordingly, removal efficiency of ATZ reached 95% in 30 min and 99.3% at 60 min with a low energy consumption of 3.08 kWh m^{-3}. Accompanied with high durability and wide applicability in pH and pollutant type, EF-ATO heightens its potential as a promising candidate for practical application in removing persistent organic pollutants. These results extend the understanding of segregation induced BIEF promoting EO process and strategies of designing robust self-supported electrodes for energy and environment application.

Author Contributions

Xue Wang: Investigation, Writing-original draft. Jia-Fang Xie: Conceptualization, Formal analysis, Visualization, Writing –review & editing, Supervision. Quan-Bao Zhao: Supervision, Funding acquisition, Writing –review & editing. Qian Sun: Resources, Methodology, Writing –review & editing.

Conflicts of interest

There are no conflicts to declare.

Acknowledgements

This work was partially supported by the National key Research & Development Program of China (2021YFA1202700), National Natural Science Foundation of China (52027815), the Youth Innovation Promotion Association CAS (2022308) to J.F. Xie. We thank Professor Xing Zhang from Anhui University for helping heterojunction construction and analysis.

References

1 S. H. Wu, H. J. He, X. Li, C. P. Yang, G. M. Zeng, B. Wu, S. Y. He and L. Lu, *Chem. Eng. J.*, 2018, **341**, 126e136.
2 X. Yu, X, Jin and N. Wang, Q. Zheng, Y. Yu, J. J. Tang, L. Wang, R. Zhou, J. Sun and L. Zhu, *Environ Int.*, 2022, 166, 107377.
3 D. Seibert, C. F. Zorzo, F. H. Borba, R. M. Souza, H. B. Quesada, R. Bergamasco and J. J. Inticher, *Sci. Total Environ.*, 2020, **748**, 141527.
4 G. R. P. Malpass, D. W. Miwa, S. A. S. Machado, P. Olivi and A. J. Motheo, *J. Hazard. Mater.*, 2006, **137,** 565-572.
5 B. P. Chaplin, *Environ. Sci. Process. Impacts.,* 2014, **16** 1182-1203.
6 S. Komtchou, A. Dirany, P. Drogui, N. Delegan, M. A. El Khakani, D. Robert and P. Lafrance, *Chemosphere.,* 2016, **157**, 79-88.
7 G. Lofrano, R. Pedrazzani, G. Libralato and M. Carotenuto, *Curr Org Chem.*, 2017, **21**, 1054-1067.
8 E. Mousset, N. Oturan, E. D. van Hullebusch, G. Guibaud, G. Esposito and M. A. Oturan, *Water Res.*, 2014, **48**, 306-316.
9 P. Zhang, L. Yu and X. W. Lou, *Angew. Chem. Int. Ed. Engl.*, 2018, **57**, 15076-15080.
10 Y. Wang, C. Shen, M. Zhang, B.-T. Zhang and Y.-G. Yu, *Chem. Eng. J.*, 2016, **296**, 79-89.
11 C. Yang, Y. Fan, P. Li, Q. Gu and X.-y. Li, *Chem. Eng. J.*, 2021, **422**, 130032.
12 X. Li, D. Shao, H. Xu, W. Lv and W. Yan, *Chem. Eng. J.*, 2016, **285**, 1-10.

View Article Online
DOI: 10.1039/D4TA03129F

13 D. Santos, M. J. Pacheco, A. Gomes, A. Lopes and L. Ciríaco, *J. Appl. Electrochem.*, 2013, **43**, 407-416.
14 S. Mestre, A. Gozalbo, M. M. Lorente-Ayza and E. Sánchez, *J. Eur. Ceram. Soc.*, 2019, **39**, 3392-3407.
15 G. Wang, Y. Liu, Y. Duan, J. Ye and Z. Lin, *Ceram. Int.*,, 2023, **49**, 15357-15364.
16 P. Parikh, M. Sina, A. Banerjee, X. Wang, M. S. D'Souza, J.-M. Doux, E. A. Wu, O. Y. Trieu, Y. Gong, Q. Zhou, K. Snyder and Y. S. Meng, *Chem. Mater.*, 2019, **31**, 2535-2544.
17 Y. Jing, S. Almassi, S. Mehraeen, R. J. LeSuer and B. P. Chaplin, *J. Mater. Chem. A.*, 2018, **6**, 23828-23839.
18 L. Chai, Q. Qu, L. Zhang, M. Shen, L. Zhang and H. Zheng, *Electrochim. Acta.*, 2013, **105**, 378-383.
19 C. Yang, S. Shang and X.-y. Li, *J. Hazard. Mater.*, 2022, **436**, 129212.
20 Z. Zhao, J. Zhang, J. Yao and S. You, *Environ. Res.*, 2022, **210**, 113004.
21 X. Wang, P. Ren, H. Tian, H. Fan, C. Cai and W. Liu, *J. Alloys Compd.*, 2016, **669**, 29-37.
22 X. Zhao, M. Liu, Y. Wang, Y. Xiong, P. Yang, J. Qin, X. Xiong and Y. Lei, *ACS Nano*, 2022, **16**, 19959-19979.
23 Z. Wu, Y. Zhao, W. Jin, B. Jia, J. Wang and T. Ma, *Adv. Funct. Mater.*, 2021, **31**, 2009070.
24 M.-C. Han, J.-H. Zhang, C.-Y. Yu, J.-C. Yu, Y.-X. Wang, Z.-G. Jiang, M. Yao, G. Xie, Z.-Z. Yu and J. Qu, *Angew. Chem. Int. Ed. Engl.*, 2024, **63**, e202403695.
25 X. Sun, S. Wang, Y. Hou, X. F. Lu, J. Zhang and X. Wang, *J. Mater. Chem. A.*, 2023, **11**, 13089-13106.
26 F.-Y. Chen, Z.-Y. Wu, Z. Adler and H. Wang, *Joule*, 2021, **5**, 1704-1731.
27 Y. Li, D. Zhang, P. Wang, J. Qu and S. Zhan, *Proc. Natl. Acad. Sci. U. S. A.*, 2024, **121**, e2407012121.
28 Y. Zhou, F. Che, M. Liu, C. Zou, Z. Liang, P. De Luna, H. Yuan, J. Li, Z. Wang, H. Xie, H. Li, P. Chen, E. Bladt, R. Quintero-Bermudez, T.-K. Sham, S. Bals, J. Hofkens, D. Sinton, G. Chen and E. H. Sargent, *Nat. Chem.*, 2018, **10**, 974-980.
29 S. Periyasamy and M. Muthuchamy, *J. Environ.*, 2018, **6**, 7358-7367.
30 X. Sun, H. Qi and Z. Sun, *Chemosphere*, 2022, **286**, 131972.
31 C. Yang, S. Shang, L. Lin, P. Wang, Z. Ye, Y. Wang, K. Shih, L. Sun and X.-y. Li, *Nat. Water*, 2024, **2**, 793-802.
32 Y. Nosaka and A. Y. Nosaka, *Chem. Rev.*, 2017, **117**, 11302-11336.

The data supporting this article have been included as part of the Supplementary Information.

View Article Online
DOI: 10.1039/D4TA03129F